

# Acoustic lens design by genetic algorithms

A. Håkansson and J. Sánchez-Dehesa\*

*Centro de Tecnología Nanofotónica and Dpto. Ingeniería Electrónica,  
Universidad Politécnica de Valencia, E-46022 Valencia, Spain.*

L. Sanchis

*Departamento de Física Teórica de la Materia Condensada,  
Facultad de Ciencias,  
Universidad Autónoma de Madrid,  
E-28049 Madrid, Spain.*

## Abstract

A survey of acoustic devices for focusing airborne sound is presented. We introduce a new approach to design high quality acoustic lenses based on arrays of cylindrical rigid scatterers in air. A population based stochastic search algorithm is used in conjunction with the multiple scattering theory to optimize a cluster of cylinders that focuses the sound in a prefixed focal point. Various lenses of different sized clusters, for different frequencies and with different focal lengths are presented. In general three focusing phenomena are remarked, focusing due to refraction, diffraction and focusing due to multiple scattering. The dependency on the frequency of the incident sound and the focal distance is analyzed indicating that higher frequencies and smaller focal distances favour larger amplifications in thin lenses based on multiple scattering. Furthermore, the robustness of a designed acoustic lens is studied, examining the focusing effect against errors in the cylinders' positions and their radius.

PACS numbers: 43.20.+g, 43.90.+v, 45.10.Db

## I. INTRODUCTION

Sonic crystals (SCs) are materials consisting of periodic distributions of acoustic scatterers in air. The periodicity in these materials give rise to sonic band gaps, a range of frequencies for which sound propagation is forbidden inside the crystal for some (pseudo gap) or all (full gap) wave vectors. These stop bands have induced various application proposals such as sound shields and acoustic filters<sup>2,3,4,5,6,7,8,9,10,11,12,13</sup>. Recently, the properties of SCs in the low frequency region, where the dispersion relation is linear, have also been of interest for device applications<sup>14,15,16,17</sup>. For these frequencies the SC behaves as a homogeneous medium with an acoustic impedance larger than air. This property has allowed the construction of two refractive devices, a convergent lens and an acoustic interferometer<sup>15</sup>. On one hand, a comprehensive study of acoustic interferometers has been reported by some of us<sup>14</sup>. On the other hand, various works<sup>16,17,18,19,20</sup> have been published about focusing sound and image formation in the light of the seminal work by Cervera *et al.*<sup>15</sup>. Different SC lenses have been proposed and a discussion has aroused about whether refraction or diffraction is the dominant mechanism for focalization<sup>17,20</sup>. Focusing sound can also be obtained by using time-reversal techniques<sup>21,22</sup>, but the discussion of these techniques is out of the scope of the present work.

The goal of this paper is to answer the following question: Which is the optimal SC structure that acts as an acoustic lens focusing the sound at a predetermined focal distance? From this point of view we will discuss what is the physics that control the focusing process in several acoustic lenses, which were optimized for different frequencies and focal distances. Our approach to the problem consists in using a population based stochastic search algorithm, specifically a genetic algorithm (GA)<sup>23</sup> in conjunction with the multiple scattering theory (MST)<sup>24</sup>. This approach has been previously used by us to design a spot-size converter in the field of two-dimensional photonic crystals<sup>25</sup>. GAs have been proved to be very efficient, especially in optimization problems having a large set of discrete parameters. To speed-up the stochastic search, here we have implemented a symmetric multiple scattering theory (SMST) that decreases the calculation time needed for predicting the scattered acoustic wave from a symmetric system.

## II. METHOD OF CALCULATION

### A. Genetic Algorithm

Evolutionary computation is a family of algorithms that are related with the optimization process used by nature itself, the evolution. The evolution is very powerful in adapting individuals to a given environment, and is able to tackle enormous complex problems with fairly simple means. Throughout generations the individuals' chromosomes (the genotypes) are mixed and new individuals with different characteristics are born. Those individuals that adapt better to the environment have the best chance of survival and hence give birth to more offspring creating a new generation more fit for survival than the previous one.

We here use one of the most popular algorithms from this family, a simple-GA, introduced by Holland<sup>23</sup>. The GAs are population based stochastic search algorithms normally used to solve discrete problems. Their functionality is based on their ability to find small parts of the individual (the solution) that reflects a good quality in the result, these fractions are called building blocks (BBs). In other words, the GA creates, mixes and finally uses these BBs to build a global optimal solution. Unfortunately this goal is not always met. If the global optimum consists of large sized BBs, the GA will have problems of constructing them because high-order BBs are very difficult to grow. These problems are referred to as GA-hard problems<sup>26</sup>. Nevertheless, this is not of great concern here since this work concentrates on the method itself and not on the algorithm. At this point, we are pleased by finding good solutions within the boundaries of the optimal.

The simple-GA works with three operators; selection, crossover and mutation that are iteratively applied to a population of individuals. The selection operator culls the population selecting better solutions over worse for mating. The mating act, which is directed by the crossover operator, mixes and constructs the BBs from two or more individuals creating new offspring. The mutation operator makes it possible for the offspring to possess new BBs that none of the parents have and is applied before passing into the next generation (i.e., the next iteration). The individual is represented by a chromosome (a digital string) that is put together by a number of binary genes coding the genotype. Each gene corresponds to one specific part of the phenotype and the corresponding value of the gene is called allele. The genotype represents one and only one phenotype that here is a cluster of rigid cylinders.

Our goal is to find which cluster focuses the sound most efficiently in a fixed predetermined focal point, under a chosen constrain or boundary condition. This cluster of cylinders can be seen as a transparent acoustic lens device. To quantitatively judge the quality of such a device, a real number is assigned to each cluster. This number is referred to as the fitness of the solution and is here calculated as the pressure in the focus if not mentioned others. One lens is better than another if its fitness is superior

To predict the fitness we need to calculate the scattered pressure field from a cluster of cylindrical scatterers. We here apply the Multiple Scattering Theory (MST) that earlier has been used by some of us with good agreement between theory and experiments<sup>14</sup>. Because the search space of the problem is very large, the GA needs to calculate the fitness for numerous individuals before converging. For example, a genotype with 50 one-bit genes could represent up to  $\sim 10^{15}$  different phenotypes. Thankfully the GA does not get near this number of fitness calculations, but it is crucial to do the fitness calculation as fast as possible. In order to speed up the fitness calculation, we apply a simple symmetric condition on the space of solutions. The scattered pressure field from a symmetric system has a mirrored symmetry with respect to the central axis. In other words, the field scattered from a cylinder off the symmetry axis is identical, only mirror reversed, as the field scattered from its symmetric associate. This means if using MST a lot of computational resources will be used to calculate the same scattered field twice for almost every cylinders in the symmetric cluster. By including this mirror symmetry in the MST the fitness calculation and the GA search are considerably accelerated.

## B. Symmetric Multiple Scattering Theory

The complete self-consistent procedure including all order of multiple scattering<sup>28</sup> that follows the seminal work of Twersky<sup>24</sup> has been reported by Chen and Ye<sup>13</sup> to study the transmission spectra of large structures. The SMST trimmed to handle symmetric systems will be introduced below.

Consider a cluster of  $N$  scatterers located at the positions  $\vec{R}_\beta (\beta = 1, 2, \dots, N)$ , all placed above or on the symmetry axis (the  $x$ -axis in Fig. 1). The complete symmetric crystal is represented if each cylinder placed off the  $x$ -axis is copied and placed at the same  $x$ -position and with the same, but negative,  $y$  coordinate. All cylinders placed below the symmetry

axis are indicated with a “+” in the index (see  $\alpha^+$  in Fig. 1).

If a symmetric external wave  $P_{sym}^{ext}$  with temporal dependence  $e^{-i\omega t}$  impinges the cluster, the total field around the cylinder  $\alpha$  is a superposition of the external field and the radiation scattered by the cluster:

$$P_\alpha(x, y) = P_{sym}^{ext}(x, y) + \sum_{\alpha \neq \beta}^N (P_\beta^{scatt}(x, y) + (1 - \delta_y) P_{\beta^+}^{scatt}(x, y)), \quad (1)$$

where  $\delta_y = 0$  if  $y_\beta \neq 0$ , and  $\delta_y = 1$  if  $y_\beta = 0$ .  $P_\beta^{scatt}$  and  $P_{\beta^+}^{scatt}$  is the field scattered by cylinder  $\beta$  and its mirror image  $\beta^+$  respectively.

These four fields can be expanded into series Bessel functions. The total incident wave to the  $\alpha$  cylinder, which consists of a superposition of the external incident wave and the scattered waves from all the other cylinders in the cluster, is expressed in terms of the Bessel function of the first kind as

$$P_\alpha(x, y) = \sum_{l=-\infty}^{\infty} (B_\alpha)_l J_l(r_\alpha \kappa) e^{il\theta_\alpha} \quad (2)$$

where  $\kappa$  is the wavenumber calculated as  $\kappa = \frac{c}{\omega}$ , where  $c$  is the sound velocity in air, i.e. 340 m/s.

The external incident plane wave, impinging to cylinder  $\alpha$  follows the same expansion principle but with the multipole coefficients  $(S_\alpha)_l$ . The scattered waves from cylinder  $\beta$  and  $\beta^+$  are expressed in a series of outgoing Hankel functions rather than regular wave functions:

$$P_\beta^{scatt}(x, y) = \sum_{l=-\infty}^{\infty} (A_\beta)_l H_l(r_\beta \kappa) e^{il\theta_\beta} \quad (3)$$

Using the multipole coefficients  $(B_\alpha)_l$ ,  $(S_\alpha)_l$ ,  $(A_\beta)_l$  and  $(A_{\beta^+})_l$  for  $P_\alpha$ ,  $P_\alpha^{ext}$ ,  $P_\beta^{scatt}$  and  $P_{\beta^+}^{scatt}$  respectively, the expression above can be cast into the following relation between coefficients:

$$(B_\alpha)_l = (S_\alpha)_l + \sum_{\beta=1}^N \sum_{l'=-\infty}^{l'=\infty} ((G_{\beta\alpha})_{ll'} (A_\beta)_{l'} + (1 - \delta_y) (G_{\beta^+\alpha})_{ll'} (A_{\beta^+})_{l'}) \quad (4)$$

$G_{\beta\alpha}$  and  $G_{\beta^+\alpha}$  being the propagator from cylinder  $\beta$  and  $\beta^+$  to  $\alpha$  respectively, whose components are

$$\begin{aligned}
(G_{\beta\alpha})_{ll'} &= (1 - \delta_{\alpha\beta}) e^{i(l'-l)\theta_{\beta\alpha}} H_{l'-l}^{(1)}(\kappa r_{\beta\alpha}) \\
(G_{\beta+\alpha})_{ll'} &= (1 - \delta_{\beta\alpha}) e^{i(l'-l)\theta_{\beta+\alpha}} H_{l'-l}^{(1)}(\kappa r_{\beta+\alpha})
\end{aligned} \tag{5}$$

where  $\delta_{\alpha\beta}$  is the Kronecker delta.

Notice that the coefficients  $S_\alpha$  are known, but  $B_\alpha$ ,  $A_\beta$  and  $A_{\beta+}$  are not. The boundary conditions at a rigid cylinder's surface states that the normal pressure gradient equals zero. This equation relates  $B_\alpha$  with  $A_\beta$  and the symmetric condition relates  $A_\beta$  with  $A_{\beta+}$ . The rigid cylinder approximation has been demonstrated to reproduce fairly well experiments made of hollow aluminum cylinders<sup>14</sup>. Now the transition matrix can be calculated and gives the proper transformation of the total incident field to cylinder  $\alpha$  expressed by the  $B_\beta$  coefficients, to the scattered field expressed using the  $A_\alpha$  coefficients:

$$(t_\alpha)_{ll'} = \frac{J_{l-1}(\kappa r_\alpha) - J_{l+1}(\kappa r_\alpha)}{H_{l+1}^{(1)}(\kappa r_\alpha) - H_{l-1}^{(1)}(\kappa r_\alpha)} \delta_{ll'} \tag{6}$$

,and the mirror symmetry ( $\theta_{\beta+} = -\theta_\beta$ ,  $r_{\beta+} = r_\beta$ ) relates  $A_\beta$  and  $A_{\beta+}$

$$\begin{aligned}
P_{\alpha+} &= \sum_{l'=-\infty}^{l'=\infty} (A_{\beta+})_{l'} H_{l'}(\kappa r_{\beta+}) e^{il'\theta_{\beta+}} = \sum_{l'=-\infty}^{l'=\infty} (A_\beta)_{l'} H_{l'}(\kappa r_{\beta+}) e^{il'(-\theta_{\beta+})} = \\
&= \sum_{l'=-\infty}^{l'=\infty} (A_\beta)_{-l'} H_{-l'}(\kappa r_{\beta+}) e^{il'\theta_{\beta+}} = \sum_{l'=-\infty}^{l'=\infty} (A_\beta)_{-l'} (-)^{l'} H_{l'}(\kappa r_{\beta+}) e^{il'\theta_{\beta+}}
\end{aligned} \tag{7}$$

$$(A_{\beta+})_{l'} = (A_\beta)_{-l'} (-)^{l'} \tag{8}$$

Introducing the coefficients from Eq. 6 and 8 in Eq. 4 will result in

$$\sum_{\beta=1}^N \sum_{l'=-\infty}^{l'=\infty} (A_\beta)_{l'} \left( \delta_{\alpha\beta} \delta_{ll'} - (t_\alpha G_{\beta\alpha})_{ll'} + (-)^{l'} (t_\alpha G_{\beta+\alpha})_{l-l'} \right) = (t_\alpha S_\alpha)_l \tag{9}$$

By truncating the angular momentum within  $|l'| \leq l_{\max}$ , Eq. 9 reduces to a linear equation where the dimension of the relevant matrix is  $N(2l_{\max} + 1) \times N(2l_{\max} + 1)$ . Note that  $N$  is not the total number of cylinders, only the cylinders placed on or above the  $x$ -axis. For a system of 100 cylinders truncated to  $l_{\max} = 3$ , the CPU-time needed to calculate the  $A$  coefficients is reduced by a factor of 4 by using the SMST instead of the standard MST. All

results presented are calculated with  $l_{\max} = 3$ . This approach is supported by the fact that no error higher than 1% was observed in any of the following calculations of the pressure field when including higher angular momentums in the series expansion. The coefficients in the transfer matrix give a good estimation of the convergence of the method. Here, the most significant matrix coefficient with an index higher than three is of the order  $\sim 1 \times 10^{-5}$ . In all optimization processes the angular momentum was truncated at  $l_{\max} = 1$  due to computational resources. Since this will not guarantee that the simulated fitness is within an proper error, a local search was later done with  $l_{\max} = 3$ . The local search was done using a GA with a much smaller population where one individual in the initial population correspond to the one with maximal fitness in the search with  $l_{\max} = 1$ . To confirm the quality of this two-step method a GA-optimization was done using  $l_{\max} = 3$  directly, with the result almost identical to the result received with the two-step optimization method, but significantly more time consuming.

Figure 2 illustrates a typical GA-run using the SMST for designing an acoustic lens. The problem is coded on 100 one-bit genes. As can be seen in the figure the algorithm has converged after approximately 50,000 fitness calculations, this equals one  $10^{-30}$ th part of the total number of phenotypes.

### III. RESULTS AND DISCUSSION

#### A. Thick lenses

Guided by recent works<sup>15,16,17,19,20</sup>, where a discussion has aroused concerning the shape of SCs devices for focusing sound, we will here as the first step in our study treat the problem of finding the optimal shape of a SC cluster for different focal distances and for different symmetry constrains.

Firstly the GA was implemented to find the optimal SC cluster, symmetric with respect to both axes, that focuses the sound on the  $x$ -axis for a fixed focal distance. To do this, the device's genotype was implemented using 10 two-bit genes, where each gene corresponds to a different layer in the cluster. The first gene on the chromosome corresponds to the central layer at  $x = 0$  and the four possible alleles of the gene (00, 01, 10, 11) code the width of this layer, 20, 18, 16 or 14 cylinders respectively. This can be interpreted as (00) keeps

the width (20 cylinders for  $x = 0$ ), (01), (10) and (11) remove one, two and three cylinder respectively, at each extreme (leaving the 18, 16 or 14 cylinders for  $x = 0$ ). The next gene on the chromosome follows this rule and is related to the two layers next to the central one. Since the crystal is symmetric the same gene code both neighboring layers. Each following gene on the chromosome relates to the next neighboring layer and the allele tells us if this layer will decrease in width (01, 10, 11) or be kept constant (00) with respect to the previous layer.

We have considered a hexagonal array of rigid cylinder with radius  $r = 2$  cm and a lattice constant  $a = 6.7$  cm. Systems having these parameters have been studied earlier both experimentally and theoretically in Refs.<sup>14,15,16,17</sup>. We also consider an incident sound plane wave traveling in the positive  $x$ -direction at 1700 Hz. This wave is perfectly symmetric with respect to the  $x$ -axis, which is the only criteria for using the SMST and it will be assumed as incident wave in all the following calculations if not mentioned others. Four different lenses for four different focal distances were designed using the GA. The same boundary conditions were applied, i.e. the central layers maximal width is 20 cylinders and the maximum number of layers equals 19 (18 layer off-axis plus the central layer on-axis). The results are shown in Fig. 3, where the amplification [in decibels (dB)] was calculated as

$$P(dB) = 20 \log \frac{|P(x_f, y_f)|}{|P_0(x_f, y_f)|}, \quad (10)$$

where  $(x_f, y_f)$  defines the focal point, and  $|P_0|$  equals the pressure measured in free space that here equals 1 for the plane wave.

The amplification in the optimized focal point for the four structures vary from 8.1 dB to 8.6 dB. The highest gain was achieved for the smallest focal length. A noteworthy observation is that the structure increases in width at the same time as the curvature of the surface decrease with longer focal length, a similar characteristic that for optical lenses and should be the case for homogenous refractive devices. This can be considered as a support of the work presented in Refs.<sup>15</sup> and<sup>16</sup>, i.e. the SC is seen as a homogeneous material and the dominant effect in focalization is due to refraction. If comparing the designed structure in Fig. 3c with the SC used in the experimental set-up in Ref.<sup>15</sup> one can clearly observe a close similarity in the curvature of the different surfaces.

The boundary conditions constraining the pool of solutions are very strong in this first



approach simplifying the optimization process. Drawn by the determination to increase the amplification of the device we lifted some of these constraints. Figure 4 shows three different devices design by the GA to maximize the focalization at  $x = 1.05$  m (the same focal distance as in Fig. 3c). The upper crystal has the most restrictions and the lower the least. This means that the number of possible solutions increases with the freedom of the GA and results in a harder problem to solve. The device in Fig. 4a is the result from a genotype including 10 three-bit genes, where each gene is related to the phenotype in a similar way as earlier. Here the three-bit gene corresponds to eight different alleles that directly code the number of cylinders in each layer; For the nine central layers in the crystal: from 20 or 19 cylinders for the allele (000) down to 6 or 5 for (111); For the ten outer layers (five to the left and five to the right) in the crystal: from 14 or 13 cylinders for the allele (000) down to no cylinders for (111). The boundary condition is set in such a way that the crystal from Fig. 3c is included in the search space and hence mark a minima for the expected optimization result. The increase in the genotype size gives rise to an increase in the total number of possible solutions from  $2^{20}$  ( $\sim 10^6$ ) in Fig. 3c to  $2^{30}$  ( $\sim 10^9$ ) in 4a. The resulting device is of the same size as in Fig. 3c but now the crystal is not lens-shaped but formed out of three thinner sections. As expected the amplification increases, from 8.1 dB to 8.3 dB.

In the next modification of the boundary condition we leave the homogeneous SC cluster and give freedom to the algorithm to introduce point-defects in the cluster. We here leave the homogenization discussion and let the GA play with the complex procedure of multiple scattering inside the cluster of scatterers, though the double symmetric condition still holds. The genotype now equals 100 one-bit genes where each one-bit gene represents the presence (1) or the absence (0) of one ( $x = 0$  and  $y = 0$ ), two ( $x = 0$  or  $y = 0$ ) or four ( $x \neq 0$  and  $y \neq 0$ ) cylinder, due to the symmetry condition. The search space is increased from  $\sim 10^9$  to  $2^{100}$  ( $\sim 10^{30}$ ) possible solutions and the optimized amplification is increased from 8.3 dB to 8.5 dB. Finally, in the last run, the symmetry with respect to the y-axis is removed and the number of one-bit genes in the chromosome is increased to 200 which result in the gigantic number of possible solution equal  $2^{200}$  ( $\sim 10^{60}$ ). Fig. 4c shows that an enhancement of sound focalization is obtained.

In principle, one would expect that giving more degrees of freedom in the inverse design process and so increasing the search space will increase the quality in the result after the

optimization, but this can be a misleading assumption. Even though the results presented here follow this supposition, it is interesting to compare the results in Fig. 4a and Fig. 4b. The qualities differ only 0.2 dB while the total number of possible solutions increases from  $\sim 10^9$  to  $\sim 10^{30}$ . Since the number of solutions increase exponentially (base 2) with the size of the chromosome it is very important to define the genotype in a good way keeping down the size of the problem and coding the BB in a way that minimizes their size. Here we have kept the GA-parameters constant during the different runs. The result in general can be enhanced trimming the GA-parameters to handle larger and harder problems. When problems of this size need to be tackled, a more advanced algorithm should be at hand, e.g. cGA (compaq GA), fmGA (fast messy GA), BOA (Bayesian Optimization Algorithm)<sup>27</sup> that are capable of dynamically finding larger sized BBs.

## B. Thin Lenses with Flat Surfaces

### 1. Five Layers lenses

Following the path of the previous analysis we now continue our study using a reduced SC framework consisting of five layers and 98 cylinders, compared to earlier nineteen layers and 371 cylinders. The degree of freedom is set at the previous highest level using 50 two-bit genes, each gene coding one cylinder. The four possible alleles of the gene are representing three different radius of the cylinders; (01): 1cm, (10):  $r=1.5$  cm and (11):  $r=2$  cm and (00): no cylinder present.

Figures 5 and 6 illustrate eight different devices for focusing the sound at eight different distances along the symmetry axis. These flat lenses represented by considerably few cylinders is perfectly competitive with the thick lenses earlier presented (e.g. compare Fig. 4c. with Fig. 6c, two lenses with the same focal distance). Although the really impacting results are for short focal lengths where the amplification reaches up to 10.3 dB. For longer focal lengths presented in Fig. 6a homogenous cluster of cylinders, where no point defect is present, can be observed as a central piece of the device. This cluster is more or less formed as a trapezoid where the shorter of the two parallel sides always is closer to the focus. That the cluster is homogeneous indicate that the focusing mechanism for this part is mostly due to refraction or diffraction of the cluster. We can clearly see in Fig. 6e that for this large

focal distance (2m) the flat lens, almost free of defects, works because of the diffraction at the borders of the cluster and the focal-spot is almost completely lost.

Figure 7 displays the eight results put together in order to show how the amplification decreases with an increase in the focal distance. This is a surprising result since lenses working due to refraction and follow Lensmaker's formula<sup>19</sup>, need to be very thick to achieve high F-numbers. The F-number, calculated as the focal length divided by the diameter of the lens, is for the structure in Fig. 5a  $\sim 0.3/1.2 = 0.25$  which is a very low number in conventional optics. It is also much lower than the SC refractive lens device reported by Cervera *et al.*<sup>15</sup> and the optimized homogeneous cluster of cylinders in Fig. 3c, which have a corresponding F-number close to one. One explanation for this is that the basic physics of the functionality is different leaving the homogenization approach were the shape of the lens is the controlling parameter, and instead using every single scatterer for bending the sound towards the focus maximizing the amplification for the set frequency.

To see how the result holds for other frequencies, Fig. 8 shows the sound amplification for eight different structures designed to maximize the pressure at the same focus (located at  $x = 0.5$  m on the symmetry axis) for eight different frequencies, from 300Hz to 1700Hz. There is a peak in the frequency spectra confining the amplification for a small range of frequencies near the optimized (indicated with a diamond symbol in the figure). In other words, a GA lens designed to focus a given frequency is not robust against small variations of the optimized frequency. A substantial decrease in the amplification for lower frequency is also observed. This result is physically understood since for larger wavelength the cluster of cylinders appear more homogeneous to the acoustic incident wave and the GA loses its capability of controlling and directing the incident acoustic wave towards the focus using single scatterers.

The previous result motivated the following question: Can we create a device that amplify the sound equally over a wide range of frequencies? This inverse problem can be solved by modifying the fitness function in such a way to include this condition in its definition. In what follows, we will see how to design a device working in the range from 1000 Hz to 2000 Hz. Thus, we have selected 6 frequencies in the range and have modify the fitness function in the optimization process accordingly. A word of caution, a homogenous amplification over the frequency spectra is not guaranteed if the average pressure of the six frequencies is simply used as the fitness for the device. To meet the homogeneous amplification criterion

one has to include the standard deviation of the six measurements. The fitness is then calculated using the following expression

$$fitness = \bar{p}(1 - s^\alpha), \quad (11)$$

where

$$\bar{p} = \frac{\sum_i |p(v_i)|}{N}, s = \sqrt{\sum_{i=1}^N (|p(v_i)| - \bar{p})^2}, \quad (12)$$

and  $\alpha$  is a positive constant. Other alternative fitness functions could be equally used.

By multiplying the average pressure with one minus the standard deviation we will end up with device that will not only max out the pressure at the focus but will have similar amplification for all six frequencies. The  $\alpha$ -constant is a factor that controls the strength of the second condition. The time needed to calculate this design is six times greater since the SMST is called six times for each fitness evaluation, one time for each frequency. The inset of Fig. 8 shows the resulting device for  $\alpha = 4$ . The corresponding amplification spectrum (circles) demonstrated that the maximal amplification is lowered from 8 dB to 4 dB, but a relative smooth amplification is accomplished in the requested range.

## 2. Nine layers lenses

To improve the results achieved for the 5 layers flat lenses we increased the number of cylinders in the SC structure. Figure 9 plots the amplification for six different GA-designed 9 layers lenses with different focal distances. In order to compare with the previous results for thinner lenses, four extra layers were added to the left of the SC structure; in this way the distance between the last layer and the focus is held constant. The comparison of Figs. 7 and 9 shows that an enhancement of approximately 2-3 dB in the amplification is obtained when introducing the extra rows of cylinders. This result gives an indication that very efficient lenses can be designed by increasing the number of scatterers.

The multifrequency focalization device was also designed with 9 layers thick clusters. The resulting device is shown in Fig. 10 together with its amplification in the range 1000 Hz-2000 Hz. Notice that an enhancement in the amplification of  $\sim 1 - 2$  dB is obtained in comparison

with the 5-layers thick device. Even if the six frequencies have a very leveled amplification we can observe oscillations in the spectra between the optimized frequencies used in the fitness function. These oscillations could be eliminated by including more frequencies in the GA optimization.

Some characteristics are remarkable when the multifrequency lenses having 5 and 9 layers are compared (see Figs. 8 and 10). First of all, the central parts of the devices are similar. They are of triangular shape with one edge directed at the focus and does not contain any point defects. This gives an indication that a crystalline cluster, free from point defects, gives rise to amplifications in a broader frequency range. And secondly, the first layers (i.e., the ones that impinges the sound first) of the central cluster mostly contain the cylinders having smaller radius while the triangular cluster is mostly made of the thickest cylinders. This characteristic results in a lower reflectance at the interface and, consequently, the transmission across the cluster is enhanced.

### C. Robustness

An issue of crucial interest is to know if the designed device is robust against changes of its parameters, such as fluctuations in the radius of the cylinders or small displacements of their position in the lattice. It has earlier been shown<sup>16</sup> that the focalization of sound using homogenous 2D SC clusters depends on the displacement of the cylinders. Here we analyzed, as a typical example, the lens shown in Fig. 5c, a flat 5 layer lens having the focus at  $x=0.5$  m for an impinging wave of 1700Hz.

Table I shows that the amplification decreases when the error in the cylinders' radius increases. The amplification is calculated for five different degrees of relative error, from 3% to 60%. Twenty structures was generated and the maximal, minimal, mean and standard deviation of these is printed out in the table. For small errors we surprisingly have a small raise in the amplification for some structures and for a relative error of 60% we still have solutions that conserve 100% of the pressure in the focus, but a mean value of 69% for the 20 structures is calculated.

The other important issue is the sensibility of the design to changes in the cylinders' positions. Table II gives the amplification for five different levels of random displacements in the lattice. The cylinders are randomly moved from their original position in the lattice

with the relative error as 1% to 15% of the lattice parameter. The quality of the device shows a rather high robustness since more than 90% of the amplitude of the pressure in the focus is conserved for a relative displacement of 12% with respect to the lattice parameter.

#### IV. SUMMARY

In this work we have examined how to solve the inverse problem of designing acoustic lenses for airborne sound by using an optimization algorithm together with a multiple scattering theory. We have introduced a symmetric multiple scattering method to speed up the search of solutions. We have presented different devices; e.g. thick lenses based on refractive effects and flat lenses based on multiple scattering phenomenon. Two lenses with flat surfaces were also designed to focus multifrequency sound waves in the range 1 kHz to 2 kHz. The robustness were also studied against either small variations of the cylinders' radius as well as displacements of their positions. We hope that these predictions motivated future experimental work that confirm the simulations. Let us stress that the procedures here introduced can be employed to design efficient sound shields, sound filters to a predetermined range of frequency, and many others acoustic devices for airborne sound. Also, its application in the range of ultrasounds seems very promising to get improved ultrasonic devices.

---

\* Electronic address: jsdehesa@upvnet.upv.es

<sup>1</sup> M. Sigalas and E. N. Economou, J. Sound Vib. **158**, 377 (1992); for a review, see M. S. Kushawaha, Recent Res. Devel. Appl. Phys. **2**, 743 (1999).

<sup>2</sup> R. Martínez-Sala, J. Sancho, J. V. Sánchez-Pérez, J. Llinares and F. Meseguer, Nature (London) **378**, 241 (1995).

<sup>3</sup> J. V. Sánchez-Pérez, D. Caballero, R. Martínez-Sala, C. Rubio, J. Sánchez-Dehesa, F. Meseguer, J. Llinares and F. Gálvez, Phys. Rev. Lett. **80**, 5325 (1998).

<sup>4</sup> Y. Y. Chen and Zhen Ye, Phys. Rev. Lett. **87**, 184301 (2001).

<sup>5</sup> D. Caballero, J. Sánchez-Dehesa, C. Rubio, R. Martínez-Sala, J. V. Sánchez-Pérez, F. Meseguer and J. Llinares, Phys. Rev. E **60**, R6316 (1999).

- <sup>6</sup> C. Rubio, D. Caballero, J. V. Sánchez-Pérez, R. Martínez-Sala, J. Sánchez-Dehesa, F. Meseguer and F. Cervera, *J. Lightwave Technol.* **17**, 2202 (1999).
- <sup>7</sup> D. Caballero, J. Sánchez-Dehesa, R. Martínez-Sala, C. Rubio, J. V. Sánchez-Pérez, L. Sanchis and F. Meseguer, *Phys. Rev. B* **64**, 064303 (2001).
- <sup>8</sup> W.M. Robertson and W.F. Ruby III, *J. Acoust. Soc. Am.* **104**, 694 (1998).
- <sup>9</sup> L. Sanchis, F. Cervera, J. Sánchez-Dehesa, J. V. Sánchez-Pérez, C. Rubio, and R. Martínez-Sala, *J. Acoust. Soc. Am.* **109**, 2598 (2001).
- <sup>10</sup> M. S. Kushwaha, *Appl. Phys. Lett.* **70**, 3218 (1997)
- <sup>11</sup> C. Goffaux, F. Maseri, J.O. Vasseur, B. Djafari-Rouhani and Ph. Lambin, *Appl. Phys. Lett.* **83**, 281 (2003)
- <sup>12</sup> J. V. Sanchez-Perez, C. Rubio, R. Martinez-Sala, R. Sanchez-Grandia and V. Gomez, *Appl. Phys. Lett.* **81**, 5240 (2002)
- <sup>13</sup> Y. Y. Chen and Zhen Ye, *Phys. Rev. E* **64**, 036616 (2001).
- <sup>14</sup> L. Sanchis, A. Håkansson, F. Cervera and J. Sánchez-Dehesa, *Phys. Rev. B* **67**, 035422 (2003).
- <sup>15</sup> F. Cervera, L. Sanchis, J. V. Sánchez-Pérez, R. Martínez-Sala, C. Rubio, F. Meseguer, C. López, D. Caballero and J. Sánchez-Dehesa, *Phys. Rev. Lett.* **88** 023902 (2002).
- <sup>16</sup> B.C. Gupta and Z. Ye., *Phys. Rev E* **67**, 036603 (2003).
- <sup>17</sup> N. Garcia, M. Nieto-Vesperinas, E. V. Ponizovskaya and M. Torres, *Phys. Rev. E* **67**, 046606 (2003).
- <sup>18</sup> A.A. Krokhin, J. Arriaga and L.N. Gumen, *Phys. Rev. Lett.* **91**, 264302 (2003).
- <sup>19</sup> C. H. Kuo and Z. Ye. <http://arxiv.org/abs/cond-mat/0312289> (2003).
- <sup>20</sup> A. Håkansson, J. Sánchez-Dehesa, F. Cervera, F. Meseguer, L. Sanchis and J. Llinares, (accepted for publication in *Phys. Rev. E*) <http://arxiv.org/abs/cond-mat/0405104> (2003).
- <sup>21</sup> M. Fink, D. Cassereau, A. Derode, C. Prada, P. Roux, M. Tanter, J-L. Thomas and F. Wu, *Rep. Prog. Phys.* **63**, 1933 (2000).
- <sup>22</sup> A. Tourin, A. Derode, and M. Fink, *Europhys. Lett.* **47**,175 (1999).
- <sup>23</sup> J. H. Holland, *Adaptation in natural and Artificial Systems* (The University of Michigan Press, Ann Arbor, 1975).
- <sup>24</sup> V. Twersky, *J. Acoust. Soc. Am.* **24**, 42 (1951).
- <sup>25</sup> L. Sanchis, A. Håkansson, D. López-Zanón, J. Bravo-Abad, and José Sánchez-Dehesa, *Appl. Phys. Lett.* **84** 4460 (2004).

- <sup>26</sup> D. E. Goldberg, Genetic Algorithms in Search, Optimization and Learning (Addison Wesley, Reading , MA, 1989).
- <sup>27</sup> D. E. Goldberg, The design of Innovation (Kluwer Academic Publishers, 2002).
- <sup>28</sup> Akira Ishimaru, Wave Propagation and Scattering in Random Media (Academic Press, 1978)



$\Delta r/r(\%)$	Max	Min	Mean	S.d.
3	1.01	0.99	1.00	<0.01
6	1.02	0.97	0.99	0.01
12	1.06	0.95	0.99	0.02
20	1.02	0.88	0.95	0.04
40	0.97	0.65	0.84	0.08
60	1.00	0.11	0.69	0.18

TABLE I: Robustness of the lens in Fig. 5c against errors ( $\Delta r$ ) of the cylinders' radius  $r$ . Twenty random structures were calculated to do a statistical representation. The columns are (from left to right); The relative error with respect to the cylinders' radius; The maximum amplification among the 20 calculated; The minimal amplification; The mean value; The standard deviation. All expressed as parts of the amplification for the perfect structure (8.3 dB).

FIG. 1: Schematic diagram showing a symmetric configuration of cylinders. The x-axis is the symmetry axis and the coordinates used in the SMST are shown in the figure. The symmetric cylinders are marked with a '+' super index.

FIG. 3: (color) (left panels) Four thick SC-lenses designed for 1700 Hz and different focal distances: (a) 0.65 m, (b) 0.85 m, (c) 1.05 m, and (d) 1.25 m. (right panels) Sound amplification in dB. The color scale used goes from blue (attenuation or dB less than 0) to green (low amplification) to red (high amplification). The maximum amplification in the focus is indicated in each plot.

FIG. 2: Diagram showing that the Genetic Algorithm converges for this 100 one-bit genes problem. The curves (corresponding scale on the left  $y$ -axis) correspond to the maximum (a) and averaged (b) fitness of the population. The grey bars (corresponding scale on the right  $y$ -axis) correspond to the standard deviation of the genotypes in the population and the black bars indicate the change in the genotype when a new maximum is found. The standard deviation is measured as the difference in the binary digit string corresponding to a chromosome.

$\Delta(\vec{r} - \vec{r}^j)/a$ (%)	Max	Min	Mean	S.d.
1	1.01	1.00	1.00	0.00
3	1.00	0.98	0.99	0.01
6	1.00	0.95	0.98	0.01
9	1.00	0.90	0.95	0.02
12	0.97	0.85	0.92	0.03
15	0.95	0.79	0.88	0.04

TABLE II: Robustness of the lens in Fig. 5c against errors ( $\Delta(\vec{r} - \vec{r}^j)$ ) in the displacement of the cylinder. Twenty random structures were calculated to do a statistical representation where each cylinder was randomly placed within a circle, centered at the lattice point, with a radius  $\Delta(\vec{r} - \vec{r}^j)/a$ . The columns are (from left to right); The relative error with respect to the lattice parameter; The maximum amplification among the 20 calculated; The minimal amplification; The mean value; The standard deviation. All expressed as parts of the amplification for the perfect structure (8.3 dB).

FIG. 4: (Left panels) Three thick SC-lenses designed to focus the sound at  $x = 1.05m$  with three different symmetry conditions (see text). The symmetry constrain is hardest for (a) and successively lifted for (b) and (c). (right panels) Sound amplification in dB. The color scale used goes from blue (attenuation or dB less than 0) to green (low amplification) to red (high amplification). The maximum amplification in the focus is indicated in each plot.

FIG. 5: (color) (Left panels) Four flat acoustic lenses, 5-layers-thick, designed for 1700 Hz and for four different focal distances a) 0.3 m, b) 0.4 m, c) 0.5 m and d) 0.7 m. Three different cylinder radius are used in the corresponding clusters: 1 cm, 1.5 cm, and 2 cm. (Right panels) Sound amplification in dB. The color scale used goes from blue (attenuation or dB less than 0) to green (low amplification) to red (high amplification). The maximum amplification in the focus is indicated in each plot.

FIG. 6: (color) (Left panels) Four flat acoustic lenses, 5-layers-thick, designed for 1700Hz and for four different focal distances a) 0.9 m, b) 1.1 m, c) 1.3 m and d) 2.0 m. Three different cylinder radius are used in the cluster; 1 cm, 1.5 cm and 2 cm . (Right panels) Sound amplification in dB. The color scale used goes from blue (attenuation or dB less than 0) to green (low aplification) to red (high amplification). The maximum amplification in the focus is indicated in each plot.

FIG. 7: Sound amplification along the symmetry axis ( $y=0$ ) for 5-layers-thick lenses designed to focus the sound at a given focal distance, see inset. Eight different acoustic lenses designed for 1700 Hz are shown. Three different cylinder radiuses are used in the corresponding lens; 1 cm, 1.5 cm, and 2 cm. The diamonds mark the  $x$ -coordinate used in the fitness calculation in the GA-run.

FIG. 8: Sound amplification (in dB) as a function of frequency for lenses designed to focus the sound at position  $x=0.5$  on symmetry axis. (right panel) The continuous lines show the behavior of eight different lenses, each one designed to focus the sound of a given frequency, which is indicated by a diamond symbol. The circles shows the behavior of an acoustic lens designed to focus a sound wave having any frequency in the range from 1000 Hz to 2000 Hz. The full circles mark the frequencies used in the fitness calculation (see Eq. (11)) (left panel) The acoustic lens, which is made of three different sized cylinders ( $r=1$  cm,  $r=1.5$  cm and  $r=2$  cm).

FIG. 9: Sound amplification along the axis of symmetry for 9-layers-thick lenses. Eight acoustic lenses designed for 1700Hz are shown. The symbol on each curve marks the focal distance used in the fitness calculation in the GA and correspond to the distants in the inset.fig9b

FIG. 10: (right panel) Sound attenuation as a function of frequency for an acoustic lens designed to focus the sound at position  $x = 0.5m$  on the symmetry axis for any frequency in the range from 1000 Hz to 2000 Hz. The black dots mark the frequencies  $\nu_i$  used in the fitness calculation (see Eq. (11)). (left panel) The corresponding structure which is made of three different sized cylinders;  $r=1$  cm,  $r=1.5$  cm and  $r=2$  cm.

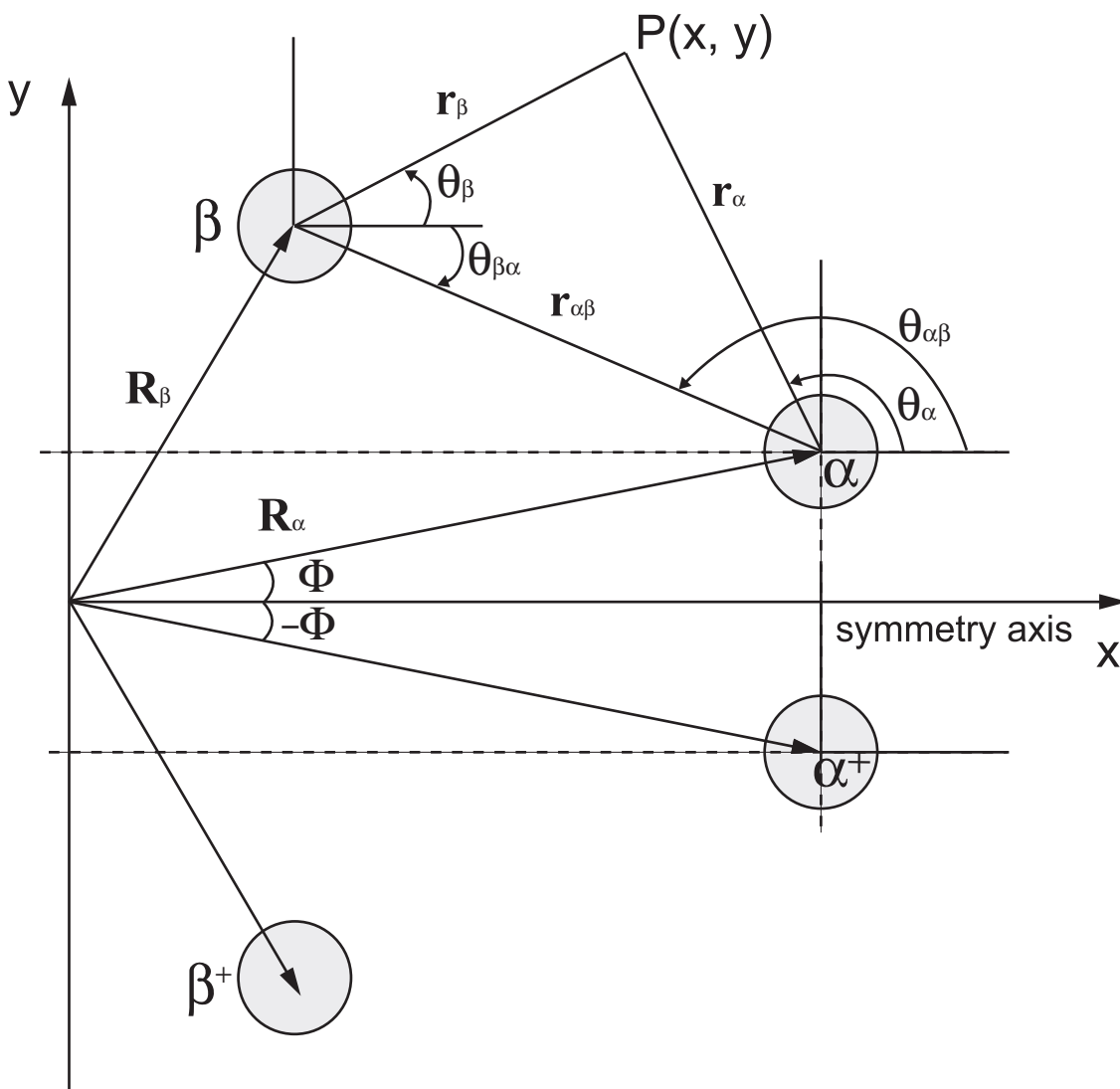


FIG. 1. A. Håkansson *et al.*

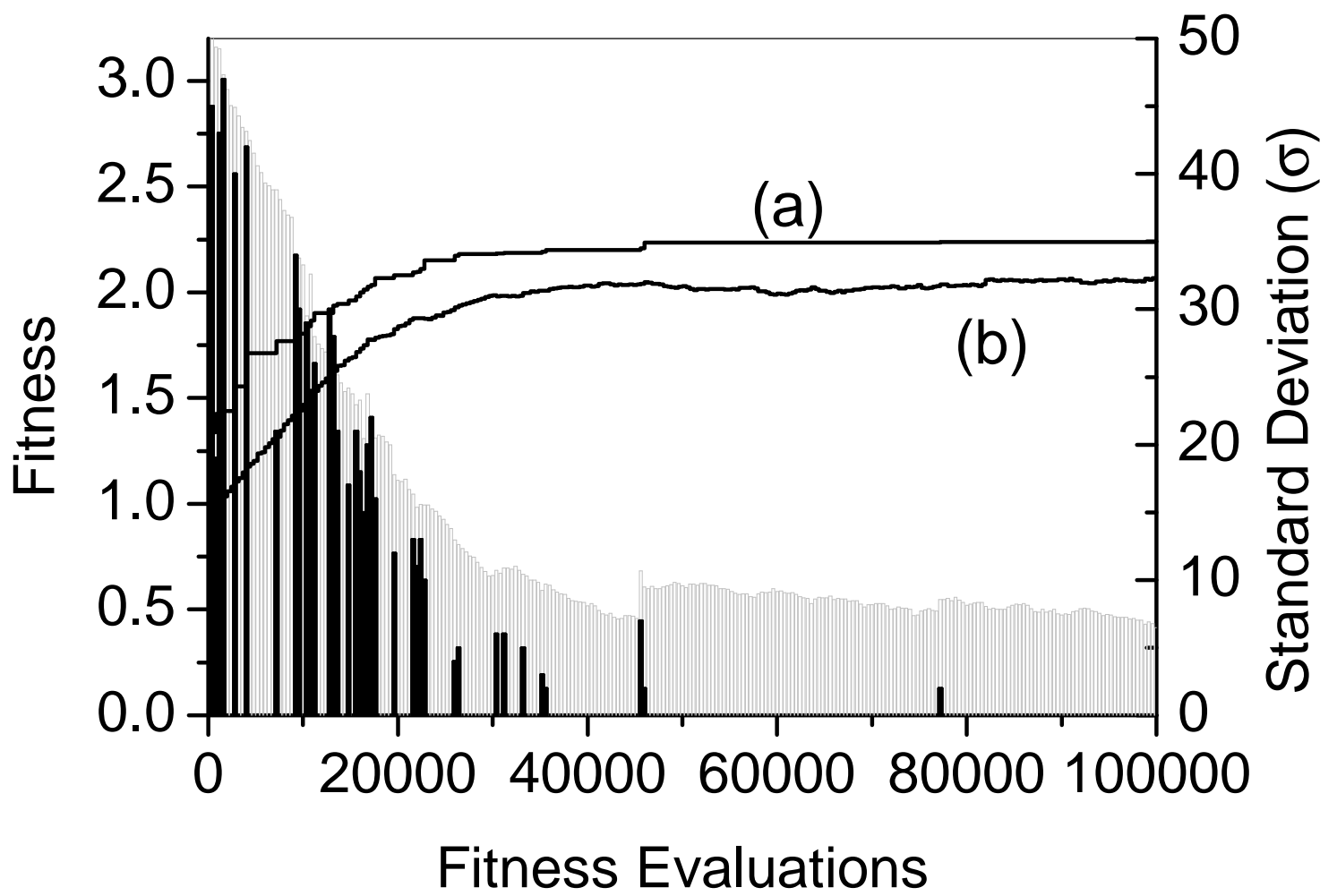


FIG. 2. Håkansson et al.

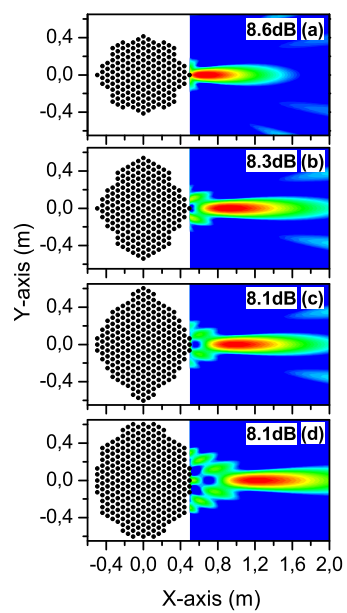


FIG. 3. Håkansson *et al.*

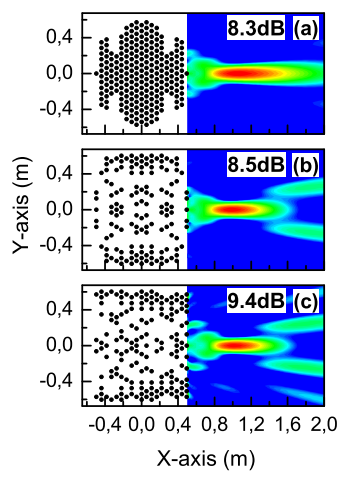


FIG. 4. A. Håkansson *et. al.*

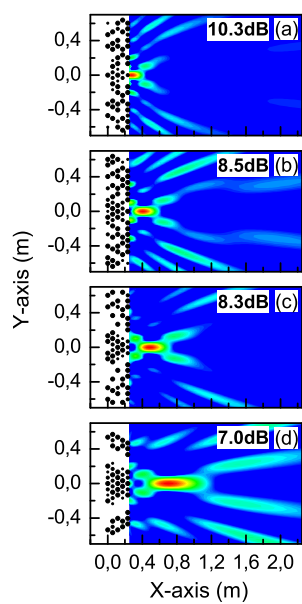


FIG. 5. Håkansson *et. al.*



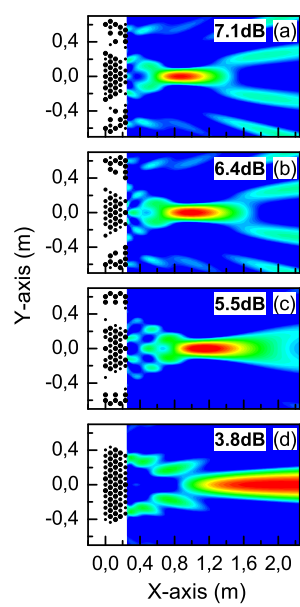


FIG. 6. Håkansson *et. al.*

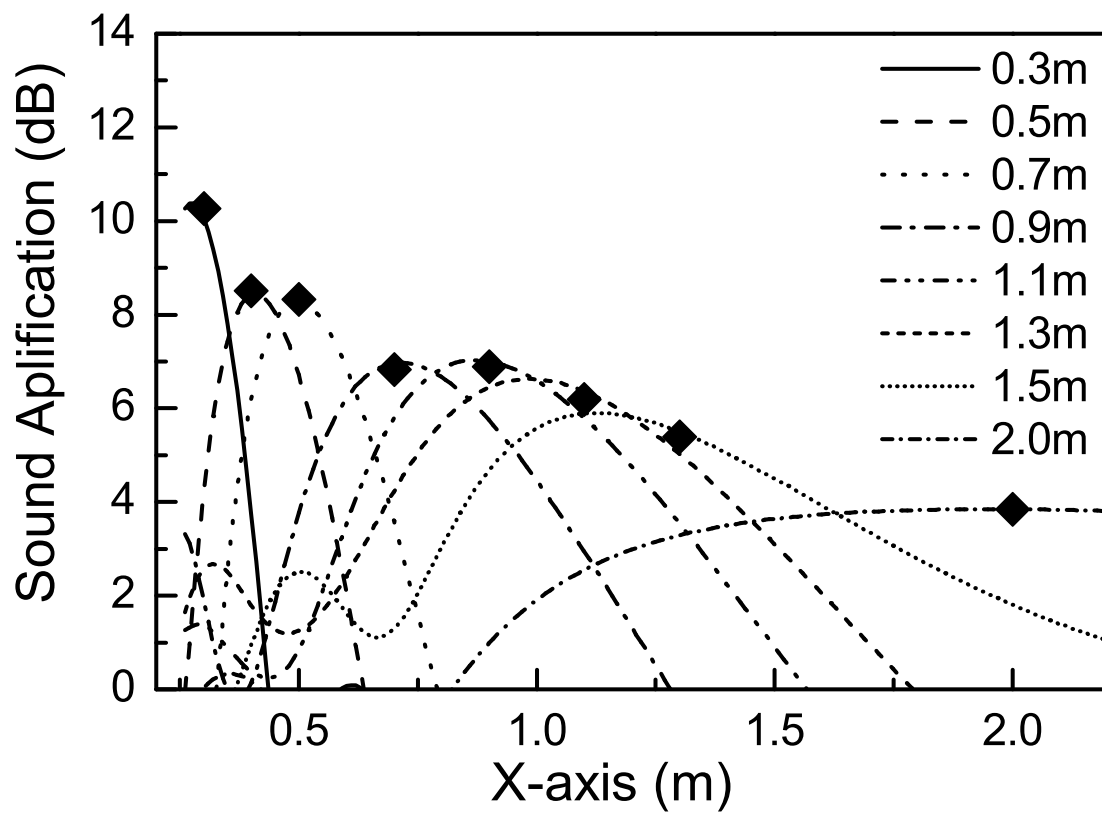


FIG. 7. A. Håkansson *et al.*

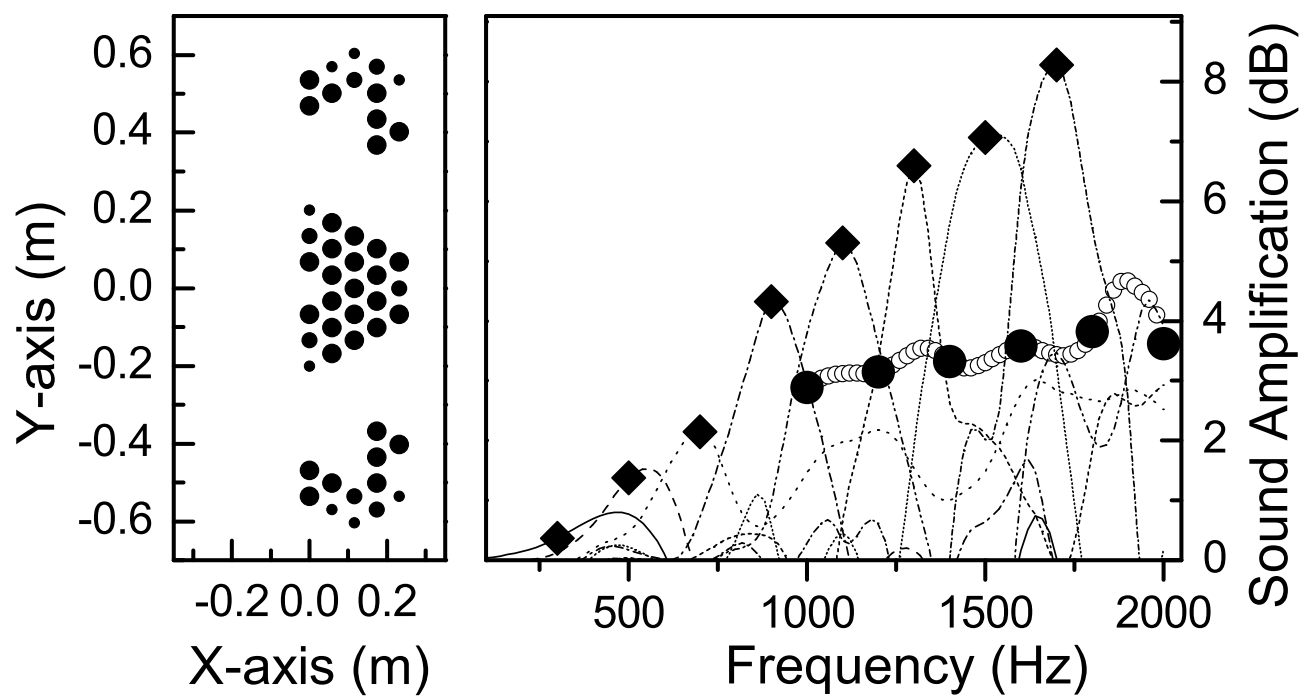


FIG. 8. A. Håkansson et al.

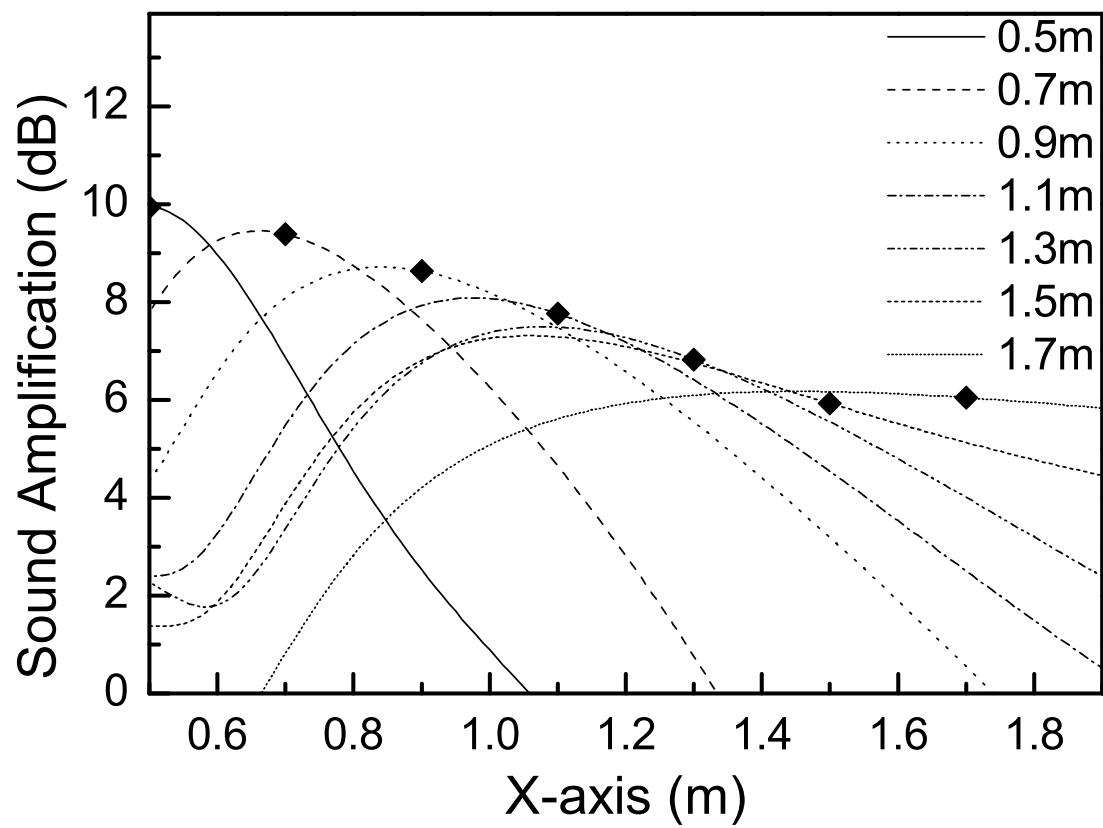


FIG. 9. A. Håkansson et al.

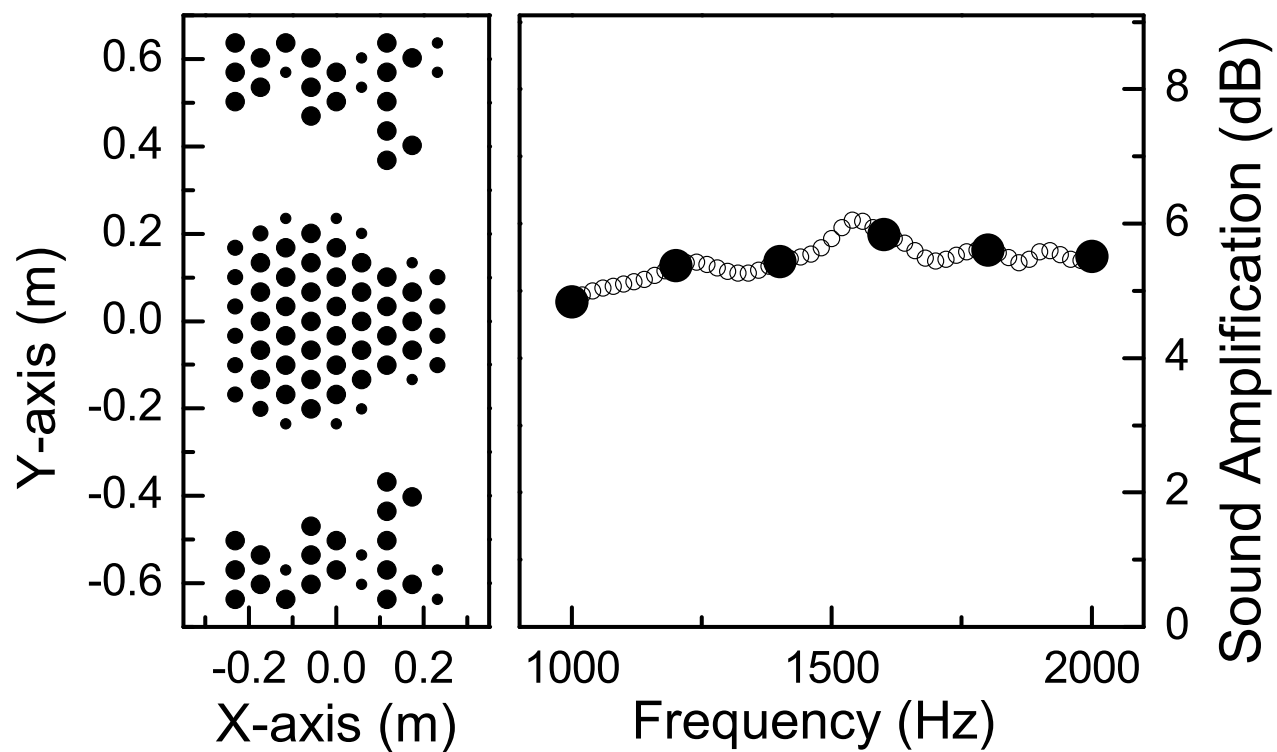


FIG. 10. A. Håkansson *et al.*